3-2009

Modeling West Antarctic ice sheet growth and collapse through the past five million years

David Pollard
Pennsylvania State University, pollard@essc.psu.edu

Robert M. DeConto
University of Massachusetts, Amherst, deconto@geo.umass.edu

Published in *Nature* **458** (19 March 19, 2009), pp. 329–332; doi: 10.1038/nature07809

Submitted August 12, 2008; accepted January 8, 2009.

Modeling West Antarctic ice sheet growth and collapse through the past five million years

David Pollard

Earth and Environmental Systems Institute, Pennsylvania State University, University Park, Pennsylvania 16802, USA;
corresponding author: email pollard@essc.psu.edu

Robert M. DeConto

Department of Geosciences, University of Massachusetts, Amherst, Massachusetts 01003, USA

Abstract
The West Antarctic ice sheet (WAIS), with ice volume equivalent to ~5 m of sea level,[1] has long been considered capable of past and future catastrophic collapse.[2, 3, 4] Today, the ice sheet is fringed by vulnerable floating ice shelves that buttress the fast flow of inland ice streams. Grounding lines are several hundred meters below sea level and the bed deepens upstream, raising the prospect of runaway retreat.[3, 5] Projections of future WAIS behavior have been hampered by limited understanding of past variations and their underlying forcing mechanisms.[6, 7] Its variation since the Last Glacial Maximum is best known, with grounding lines advancing to the continental-shelf edges around ~15 kyr ago before retreating to near-modern locations by ~3 kyr ago.[8] Prior collapses during the warmth of the early Pliocene epoch[9] and some Pleistocene interglacials have been suggested indirectly from records of sea level and deep-sea-core isotopes, and by the discovery of open-ocean diatoms in subglacial sediments.[10] Until now,[11] however, little direct evidence of such behavior has been available. Here we use a combined ice sheet/ice shelf model[12] capable of high-resolution nesting with a new treatment of grounding-line dynamics and ice-shelf buttressing[5] to simulate Antarctic ice sheet variations over the past five million years. Modeled WAIS variations range from full glacial extents with grounding lines near the continental shelf break, intermediate states similar to modern, and brief but dramatic retreats, leaving only small, isolated ice caps on West Antarctic islands. Transitions between glacial, intermediate and collapsed states are relatively rapid, taking one to several thousand years. Our simulation is in good agreement with a new sediment record (ANDRILL AND-1B) recovered from the western Ross Sea,[11] indicating a long-term trend from more frequently collapsed to more glaciated states, dominant 40-kyr cyclicity in the Pliocene, and major retreats at marine isotope stage 31 (~1.07 Myr ago) and other super-interglacials.

Large-scale modeling of the WAIS requires an ice-sheet model that combines the flow regimes of grounded and floating ice efficiently enough to allow simulations of ~10^5 yr or more. This is challenging, because the scaled equations for the two regimes are very different, and near the grounding line they interact in a boundary-layer zone that affects the large-scale dynamics.[5] More rigorous higher-order flow models without separate scalings are currently too computationally expensive for long-term continental applications.[13] Our approach simply combines the scaled sheet and shelf equations,[12] while capturing grounding-line effects by imposing a new mass-flux condition.[5] Other standard model components predict variations in ice thickness, ice temperatures, and bedrock elevation below the ice (see Methods).

The multi-million-year timescales considered here are beyond the capability of most climate models to provide the necessary time-continuous forcings required by the ice sheet model. Instead we use techniques similar to those used in previous studies[6, 7] and drive the model with simple parameterizations of surface mass balance, air temperature and specified sea level. A new parameterization of sub-ice-shelf ocean melt based on modern observations[14, 15, 16] accounts for changes in the shape of coastlines and distance from the ice edge to open ocean[17] (see Methods).

Before considering long-term simulations, it is helpful to examine the link between equilibrated ice-sheet states and the strength of various forcing mechanisms (Figure 1) representative of extreme interglacial (left of graphs), modern interglacial (middle) and full glacial (right) conditions. In between the values shown, each forcing is linearly interpolated along the x axis. This closely approximates how they co-vary in long-term simulations, but not exactly due to independent influences of $\delta^{18}O$ and austral insolation (see below). The envelopes of ocean-melt values are chosen so that complete WAIS collapse and full glacial expansion are just attained.

Figure 1a indicates a smoothly varying response from intermediate to large WAIS sizes, with sharper transitions into and out of extreme interglacials (collapses), and also back from full glacial to intermediate states. This behavior is seen in long-term simulations and animations (Supplementary Videos 1, 2), with rapid transitions taking from one to several thousand years. The whole range of Antarctic states in the model is more or less "one-dimensional," that is, the Ross, Weddell and Amundsen Sea sectors of the WAIS usually retreat and expand in unison, resulting in just one type of configuration for a given total ice volume. This suggests that the broad-scale Plio-Pleistocene history of the WAIS is represented at the ANDRILL AND-1B drill site[11], and persistent absence of a Ross ice shelf is indeed indicative of major WAIS retreat.

The relative importance of individual forcing mechanisms is shown in Figure 1b. For modern to extreme interglacial conditions, changes in surface climate and sea level are relatively small, while changes in ocean melt are dominant via their effect on ice-shelf buttressing. For modern to glacial conditions, a combination of ocean-melt and sea-level changes is needed to produce realistic WAIS expansion.[6, 7] Changes in precipitation and surface temperature have significant, but largely canceling, effects: without reduced precipitation in cooler climates, glacial volumes are too large ("no ΔP," Figure 1b); without the effects of cooler surface temperatures on internal ice temperatures, viscosities and basal sliding, glacial ice flows too easily and volumes are too small ("no ΔT," Figure 1b).

A five-million-year simulation (Figure 2) is performed from the early Pliocene to present, with the long-term variation of each forcing mechanism parameterized largely as a function of deep-sea-core $\delta^{18}O$ (reference 18). Sea level over most of this interval is dominated by Northern Hemispheric ice volume, and can be readily prescribed in proportion to $\delta^{18}O$. The responses of Antarctic surface temperature and precipitation to Pleistocene glacial cycles are also reasonably constrained by climate studies and observations, and we adapt established

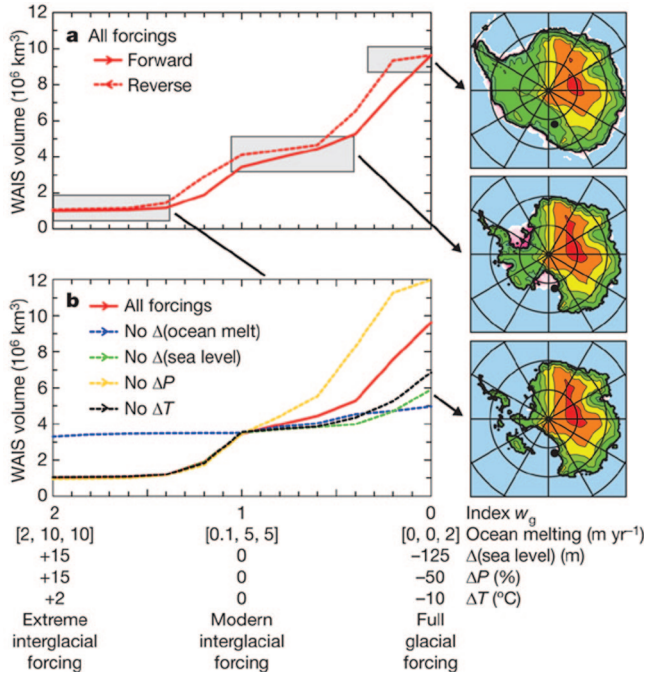

Figure 1. Equilibrium West Antarctic ice volumes versus specified forcing, and ice-sheet configurations. Left panels, ice volumes. The four forcing mechanisms are sub-ice-shelf oceanic melting and departures of sea level, annual precipitation ΔP and temperature ΔT from present. The three sets of forcing values represent climates for extreme interglacial (left), modern interglacial (middle), and full glacial (right). In between, each forcing is linearly interpolated along the x-axis (w_g, see equation (6) in Methods). The triplets of sub-ice oceanic melt rates are for protected, exposed-shelf, and deep-ocean regions—$[M_p, M_e, M_d]$, equations (7) and (8) in Methods. **a)** All forcing mechanisms changed together. Solid (dashed) curves are generated with ice sheets initialized from prior solutions representing cooling (warming) trends. The slight difference between the two curves contrasts with the much larger hysteresis of East Antarctica, where surface melt and not sub-ice-shelf melt is the dominant ablation process.[32] **b)** With one mechanism held constant at its modern value, and all others changed. Right panels, ice sheet configurations representative of the three climatic states, with the black dot showing the location of the ANDRILL AND-1B drill site.[11]

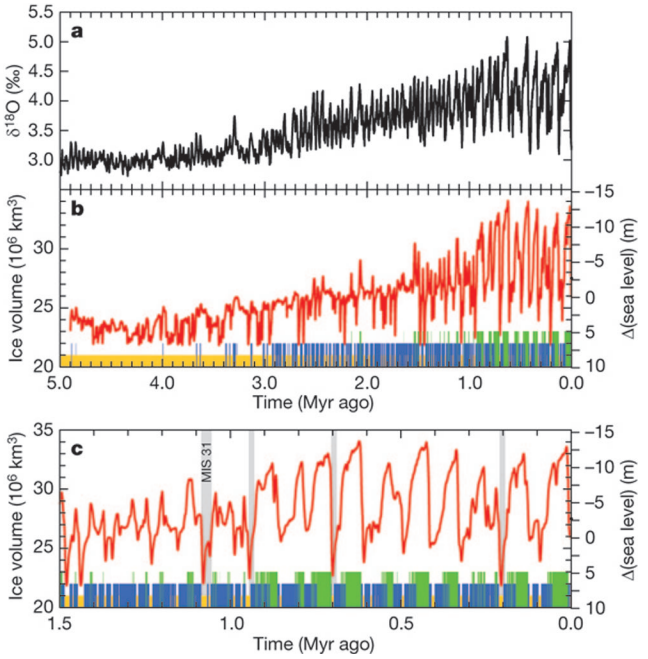

Figure 2. Simulated total Antarctic ice volume over the past five million years. **a**) Stacked deep-sea-core benthic $\delta^{18}O$ (reference 18). **b)** Total Antarctic ice volume (red line) in a long-term simulation with variations of sub-ice melt and other forcings parameterized mainly from the deep-sea-core $\delta^{18}O$ record. Equivalent changes in global sea level are shown on the right, accounting for the fraction of grounded ice above sea level compared to that below sea level.[1] Bars along the x-axis indicate conditions at a single location (78.0° S, 169.4° E), shifted one grid box to the east of AND-1B[11] to avoid poorly resolved Ross Island shorelines (yellow, open ocean; blue, floating ice shelf; green, grounded ice). Yellow and blue/green here correspond to the AND-1B diatomite (yellow) and diamictite (green) intervals in Figure 2 of reference 11. **c)** As **b** but with the time axis expanded over the past 1.5 Myr. Grey shading indicates simulated super-interglacials, beginning with MIS 31.[21]

parameterizations using $\delta^{18}O$ and austral insolation as inputs (equations (1) and (2) in Methods).

Factors controlling past variations of oceanic sub-ice melt on ~10^4 yr timescales are less certain. Sub-ice oceanic melting is affected in part by circum-Antarctic deep-water (CDW) warmth and its incursions onto continental shelves.[19] We argue that CDW and sub-ice melt have been mainly controlled by far-field climatic influences that vary in step with Northern Hemispheric glacial–interglacial cycles (see Methods). Without identifying the explicit link (which may involve atmospheric CO_2, meridional overturning circulation, sea level, or other global-scale teleconnections), we hypothesize that temporal variations of Antarctic sub-ice ocean melt rates are represented by records that correlate with Northern Hemispheric glacial variations, that is, deep-sea-core $\delta^{18}O$ (equations (6)–(8) in Methods). A minor additional influence on sub-ice melt from austral summer orbital insolation anomalies[20] is also needed to produce precessional cyclicity like that observed during marine isotope stage 31 (MIS 31) around 1 Myr ago.[11, 21] Our forcing is warmest during the early Pliocene warm period (~5 to ~3 Myr ago) due to light $\delta^{18}O$ values at that time; however, the parameterizations are based more on Pleistocene variations, and may not fully represent the warm Pliocene if unique processes (for example, persistent El Niño)[9] were involved.

With long-term forcing variations mainly following deep-sea-core $\delta^{18}O$ (ref. 18), the ice-sheet model is continuously integrated over the past 5 Myr (Figure 2). Except for small variations along the Wilkes margin[22] and in inlets such as Prydz bay,[23] East Antarctica is stable throughout the simulation and nearly all of the ice-volume variability is due to West Antarctica. Several key aspects of the model time series agree with the AND-1B core.[11] There is an overall progression from predominantly smaller WAIS sizes to larger. Furthermore, intervals of WAIS collapse with little or no marine ice are much more common from ~5 to 3 Myr ago, which is consistent with intervals in the drillcore dominated by diatomaceous sediments indicating warmer sea surface temperatures, little or no summer sea ice, and an open marine Ross embayment.[11] In fact, the two thickest diatomaceous intervals in the core, between ~4.3 and 3.4 Myr ago, correspond to the period with the most frequent and prolonged WAIS collapses simulated by the model. These collapses could well be continuous if additional Pliocene warm-period forcing was added.[9] After 3 Myr ago, there are longer intervals with modern-to-glacial ice volumes, that is, with ice-shelf or grounded-ice cover at or near the AND-1B site (Figure 2), again in rough agreement with the increasing predominance of diamictite after 3 Myr ago indicating overriding ice or a proximal grounding zone.[11]

Brief WAIS super-interglacial collapses occur after 3 Myr ago but with decreased frequency. In some cases, these precisely match the thinner diatomaceous intervals in the AND-1B core, including the well-dated MIS 31 event at 1.07 Myr ago.[11, 21] The large 100-kyr fluctuations of the past million years are similar to those modeled in earlier studies.[6, 7, 17] The last retreat of WAIS from ~15 kyr ago to the present roughly matches the observed retreat of Ross Sea grounding lines,[24, 25] and is particularly realistic with modifications described in Supplementary Information section 6.

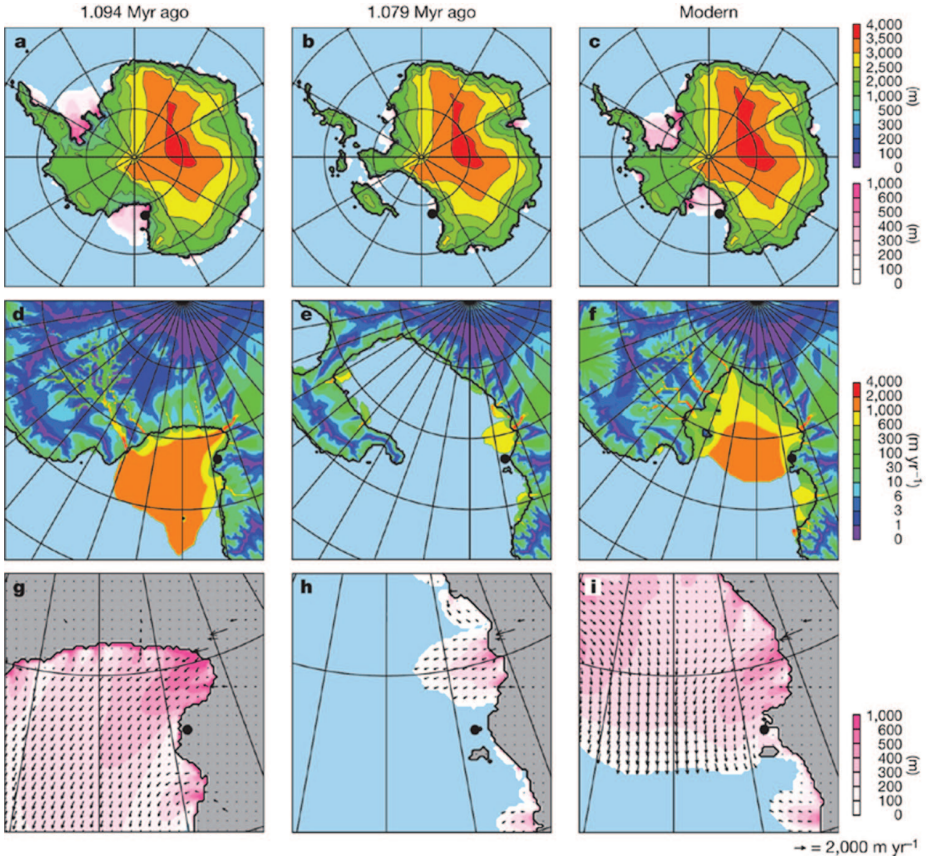

Figure 3. Snapshots at particular times from the long-term simulation in Figure 2. Shown are 1.094 Myr ago, 1.079 Myr ago (MIS 31 retreat) and modern. **a–c)** Grounded ice elevations and floating ice thicknesses, shown respectively (in m) by upper and lower color scale on right. **d–f)** Surface ice speeds (m yr^{-1}), from higher-resolution (10 km) nested runs over the Ross embayment for the same three times, showing the whole nested domain. **g–i)** Floating ice thicknesses (m) and velocity vectors from the nested simulations, enlarged over the western Ross embayment. Vectors are shown only every third grid point for clarity. The location of AND-1B is shown by the black dot.

The model predicts several major WAIS collapses during Pleistocene interglacials (Figure 2c), at times when $\delta^{18}O$ minima coincide with strong austral summer insolation anomalies. The simulated collapse at MIS 31 corresponds well with core evidence,[11, 21] both in terms of timing and magnitude, but more recent collapses (for example, ~200 kyr ago) do not always coincide with the late-Pleistocene interglacials (~125 kyr ago and ~400 kyr ago) usually suspected of harboring such events.[10, 26, 27] Thus, while the total number of collapses is reasonable, their sometimes imprecise timings may reflect the limitations of our simple forcing parameterizations, including uncertainties in the 40-kyr phase relationship of Antarctic sub-ice melt to deep-sea-core $\delta^{18}O$ records, and the influence of local orbital insolation forcing. Although the model clearly captures the overall ~40-kyr periodicity seen in the AND-1B record, the precise phasing between Antarctic ice sheet variations and Northern Hemispheric climate changes remains uncertain. In some instances, the timing of our simulated super-interglacials may be an artifact of the phasing between the imposed $\delta^{18}O$ and austral summer insolation forcings. Recent observational and modeling studies on the relative timing of Northern Hemisphere ice volume variations, ocean meridional overturning and orbital forcing[28, 29, 30] are pertinent to this issue, but with no clear consensus to date. These relationships could also be explored in future work with global climate models in combination with regional circum-Antarctic and sub-ice-shelf ocean modeling,[14, 19] to better ascertain the effects of Northern Hemispheric glacial cycles, orbital forcing and greenhouse gas concentrations on regional Antarctic conditions.

To better focus on the Ross embayment and the AND-1B site,[11] we ran higher-resolution (10 km) nested ice sheet-shelf simulations for particular times, with boundary conditions at the domain edges obtained from the long-term all-Antarctic simulation. Figure 3 illustrates a wide range of WAIS states, from weak glacial, full WAIS collapse, to modern conditions. The modern network and behavior of Siple Coast ice streams and Transantarctic outlet glaciers is well resolved (Figure 3f), with some ice streams stagnating and re-activating over the several thousand years of the nested run[31] (Supplementary Videos 3 and 4). Ross ice shelf velocities are also similar to observations, as is the central streamline dividing Siple (West Antarctic) and Transantarctic (East Antarctic) ice.[31] The finer ice grid resolves the general ice flow around Ross Island, although the details of flow are not fully resolved within the narrow confines of McMurdo Sound containing AND-1B and other drill sites.[11, 21] When shelf ice is present at AND-1B (Figure 3i), offshore flow just to the east is always northward, with ice originating from major Transantarctic outlet glaciers to the south (Byrd, Skelton, Mulock). This offshore flow pattern and its Transantarctic provenance prevail whenever there is shelf ice around Ross Island.

The dominant regional control is the overall strength of sub-ice oceanic melting in the Ross embayment, which causes both Siple- and Transantarctic-sourced ice to recede or advance in concert over the eastern and western sides of the embayment, respectively. It is very rare for one type or the other to dominate. Thus, although the provenance of shelf ice around Ross Island may be insensitive to the overall WAIS state, the basic presence or absence of shelf ice at the AND-1B site[11] is a good qualitative indicator of maxima and minima in WAIS ice volume (Figure 2). Other sites not yet cored in the central Ross embayment may offer even better potential for uniquely identifying times of WAIS collapse (Supplementary Figure 3). These simulations show how local observables in the AND-1B and other cores relate to overall WAIS evolution.

In particular, our results imply that the presence or absence of grounded or floating ice in the vicinity of McMurdo Sound is indeed linked to WAIS ice volume, and that open-water conditions in the Ross Sea are indicative of partial to complete collapse of the WAIS.

Some of our results are independent of the parameterized temporal variations in long-term forcing. For example, the estimated magnitudes of sub-ice oceanic melt rates needed to produce full WAIS amplitudes (Figure 1 and Methods) form a point of reference for future modeling. Another independent result is the tendency for the WAIS to experience relatively rapid transitions within one to a few thousand years, as forcing is smoothly varied. This includes transitions into and out of collapsed states, and from full glacial to modern-like ice extents. A collapse from modern conditions occurs when sub-ice ocean melting increases from 0.1 to 2 m yr^{-1} under shelf interiors, and from 5 to 10 m yr^{-1} near exposed shelf edges (M_p and M_e respectively, in equations (3), (7) and (8) in Methods). Recent melt rates under small Antarctic ice shelves are inferred to be increasing dramatically.[15, 16] The relationship between sub-ice melt rates and ocean temperatures is just beginning to be explored,[19] but those data[15, 16] and simplified modeling[14] suggest relationships on the order of 10 m yr^{-1} °C^{-1} for smaller shelves, and 0.4 m yr^{-1} °C^{-1} for whole-shelf averages under the major Ross and Filchner-Ronne shelves. Dividing our interior-melt (M_p) increase of 1.9 m yr^{-1} by the latter sensitivity of 0.4 m yr^{-1} °C^{-1} suggests that the WAIS will begin to collapse when nearby ocean temperatures warm by roughly 5 °C. Global climate and regional ocean modeling is needed to predict when and if future ocean temperatures and melt rates under the major Antarctic ice shelves will increase by these amounts, and if so, for how long.

Methods Summary

The scaled dynamical equations for sheet flow (shallow ice approximation) and shelf flow can be combined heuristically.[12] However, for efficiency in these long-term simulations, they are applied separately depending on whether ice is grounded or floating. Despite this simplification and coarse grids, the effects of the grounding-line boundary layer are captured by imposing a mass-flux condition across the grounding line following reference 5, which sets ice velocities there as a function of ice thickness. To include important effects of ice-shelf buttressing, the imposed grounding-line velocities are reduced depending on the ratio of longitudinal stress to its free-floating value[5] (see Supplementary Information). The model also contains three other standard components: (1) an ice-mass advection equation predicting ice thickness and accounting for surface accumulation minus ablation and basal melt, (2) an ice temperature equation including horizontal advection, vertical diffusion and shear heating, and (3) a bedrock elevation equation with local relaxation towards isostatic equilibrium and elastic lithospheric flexure.[6, 7] There is no explicit basal hydrology, other than allowing basal sliding only where the bed is at the melt point.

Equilibrium ice-free topography and bathymetry are prescribed from the modern BEDMAP database,[1] by removing all ice and allowing the bed to rebound isostatically. Prescribed basal sliding coefficients crudely represent the likely spatial distribution of deformable sediment versus hard bedrock, that is, sediment where the ice-free rebounded topography is below sea level (mostly WAIS) and bedrock where above (mostly East Antarctic ice sheet). In addition, intermediate basal stiffness is prescribed in the Pine Island/Thwaites drainage sector and Transantarctic inlets below sea level, to improve modern grounding-line locations and glacier velocities there. Past surface mass balance and sub-ice-shelf oceanic melting are parameterized using deep-sea-core $\delta^{18}O$ and orbital insolation variations (see Methods). The model is run on a polar stereographic grid, with 40 km resolution for continental and 10 km for nested experiments.

References

1. Lythe, M. B. *et al.* BEDMAP: A new ice thickness and subglacial topographic model of Antarctica. *J. Geophys. Res. Solid Earth* 106 (B6) 11335–11351 (2001)
2. Mercer, J. H. West Antarctic ice sheet and CO_2 greenhouse effect: A threat of disaster. *Nature* 271, 321–325 (1978)
3. Weertman, J. Stability of the junction of an ice sheet and an ice shelf. *J. Glaciol.* 13, 3–11 (1974)
4. Oppenheimer, M. & Alley, R. B. The West Antarctic ice sheet and long term climate policy – An editorial comment. *Clim. Change* 64, 1–10 (2004)
5. Schoof, C. Ice sheet grounding line dynamics: Steady states, stability, and hysteresis. *J. Geophys. Res.* 112 F03S28 doi:10.1029/2006JF000664 (2007)
6. Ritz, C., Rommelaere, V. & Dumas, C. Modeling the evolution of Antarctic ice sheet over the last 420,000 years: Implications for altitude changes in the Vostok region. *J. Geophys. Res.* 106 (D23) 31943–31964 (2001)
7. Huybrechts, P. Sea-level changes at the LGM from ice-dynamic reconstructions of the Greenland and Antarctic ice sheets during the glacial cycles. *Quat. Sci. Rev.* 21, 203–231 (2002)
8. Anderson, J. B. *Antarctic Marine Geology* (Cambridge Univ. Press, 1999)
9. Ravelo, A. C. *et al.* Regional climate shifts caused by gradual global cooling in the Pliocene epoch. *Nature* 429, 263–267 (2004)
10. Scherer, R. P. Quaternary and Tertiary microfossils from beneath Ice Stream-B – Evidence for a dynamic West Antarctic Ice-Sheet History. *Glob. Planet. Change* 90, 395–412 (1991)
11. Naish, T. *et al.* Obliquity-paced, Pliocene West Antarctic ice sheet oscillations. *Nature* 458 (March 19, 2009), pp. 322-329; doi:10.1038/nature07867 ; http://digitalcommons.unl.edu/geosciencefacpub/185/
12. Pollard, D. & DeConto, R. M. in *Glacial Sedimentary Processes and Products* (eds. Hambrey, M., Christoffersen, P., Glasser, N. & Hubbard, B.) 37–52 (Spec. Publ. 39, International Association of Sedimentologists, Blackwell Publishing, 2007)
13. Pattyn, F. A new three-dimensional higher-order thermomechanical ice sheet model: Basic sensitivity, ice stream development, and ice flow across subglacial lakes. *J. Geophys. Res.* 108 (B8). 2382 doi:10.1029/2002JB002329 (2003)
14. Beckmann, A. & Goose, H. A parameterization of ice shelf-ocean interaction for climate models. *Ocean Model.* 5, 157–170 (2003)
15. Rignot, E. & Jacobs, S. S. Rapid bottom melting widespread near Antarctic ice sheet grounding lines. *Science* 296, 2020–2023 (2002)
16. Shepherd, A., Wingham, D. & Rignot, E. Warm ocean is eroding West Antarctic Ice Sheet. *Geophys. Res. Lett.* 31 L23402 doi:10.1029/2004GL021106 (2004)
17. Philippon, G. *et al.* Evolution of the Antarctic ice sheet throughout the last deglaciation: A study with a new coupled climate - north and south hemisphere ice sheet model. *Earth Planet. Sci. Lett.* 248, 750–758 (2006)
18. Lisiecki, L. E. & Raymo, M. E. A. Pliocene-Pleistocene stack of 57 globally distributed benthic $\delta^{18}O$ records. *Paleoceanography* 20 PA1003 doi:10.1029/2005PA001153 (2005)
19. Holland, P. R. & Jenkins, A. The response of ice shelf basal melting to variations in ocean temperature. *J. Clim.* 21, 2558–2572 (2008)
20. Laskar, J. *et al.* A long-term numerical solution for the insolation quantities of the Earth. *Astron. Astrophys.* 428, 261–285 (2004)
21. Scherer, R. P. *et al.* Antarctic records of precession-paced insolation-driven warming during early Pleistocene Marine Isotope Stage 31. *Geophys. Res. Lett.* 35 L03505 doi:10.1029/2007GL032254 (2008)
22. Hill, D. J., Haywood, A. M., Hindmarsh, R. C. A. & Valdes, P. J. in *Deep Time Perspectives on Climate Change: Marrying the Signals from Computer Models and Biological Proxies* (eds. Williams, M., Haywood, A. M., Gregory, F. J. & Schmidt, D. N.) 517–538 (Micropaleontological Society Special Publications, Geological Society, 2007)
23. O'Brien, P. E. *et al.* Late Neogene ice drainage changes in Prydz Bay, East Antarctica and the interaction of Antarctic ice sheet evolution and climate. *Palaeogeogr. Palaeoclimatol. Palaeoecol.* 245, 390–410 (2007)
24. Conway, H. *et al.* Past and future grounding-line retreat of the West Antarctic Ice Sheet. *Science* 286, 280–283 (1999)
25. McKay, R. M. *et al.* Retreat history of the Ross Ice Sheet (Shelf) since the Last Glacial Maximum from deep-basin sediment cores around Ross Island. *Palaeogeogr. Palaeoclimatol. Palaeoecol.* 260, 245–261 (2008)
26. Hearty, P. J. *et al.* Global sea-level fluctuations during the Last Interglaciation (MIS 5e). *Quat. Sci. Rev.* 26, 2090–2112 (2007)
27. Raynaud, D. *et al.* in *Earth's Climate and Orbital Eccentricity: The Marine Isotope Stage 11 Question* (eds. Droxler, A. W., Poore, R. Z. & Burckle, L. H.) 27–40 (American Geophysical Union, 2003)
28. Lisiecki, L. E., Raymo, M. E. & Curry, W. B. Atlantic overturning responses to Late Pleistocene climate forcings. *Nature* 456, 85–88 (2008)
29. Huybers, P. & Denton, G. Antarctic temperature at orbital timescales controlled by local summer duration. *Nature Geosci.* 1, 787–792 (2008)
30. Kawamura, K. *et al.* Northern Hemisphere forcing of climatic cycles in Antarctica over the past 360,000 years. *Nature* 448, 912–916 (2007)
31. Hulbe, C. & Fahnestock, M. Century-scale discharge stagnation and reactivation of the Ross ice streams, West Antarctica. *J. Geophys. Res.* 112 F03S27 doi:10.1029/2006JF000603 (2007)
32. Pollard, D. & DeConto, R. M. Hysteresis in Cenozoic Antarctic ice sheet variations. *Glob. Planet. Change* 45, 9–21 (2005)
33. Huybrechts, P. Glaciological modelling of the late Cenozoic East Ant-

arctic Ice Sheet: Stability or dynamism? *Geogr. Ann. A* 75, 221–238 (1993)
34. Huybrechts, P. *Report of the Third EISMINT Workshop on Model Intercomparison* (European Science Foundation, 1998)
35. Marshall, S. J. & Clarke, G. K. C. Ice sheet inception: Subgrid hypsometric parameterization of mass balance in an ice sheet model. *Clim. Dyn.* 15, 533–550 (1999)
36. Macayeal, D. R. & Thomas, R. H. The effects of basal melting on the present flow of the Ross Ice Shelf, Antarctica. *J. Glaciol.* 32, 72–86 (1986)
37. Dinniman, M. S., Klinck, J. M. & Smith, W. O. Influence of sea ice cover and icebergs on circulation and water mass formation in a numerical circulation model of the Ross Sea, Antarctica. *J. Geophys. Res* 112 C11013 doi:10.1029/2006JC004036 (2007)

Acknowledgments

We thank T. Naish and R. Powell for discussions on this work, and P. Barrett for comments on the manuscript. This work was funded by the US National Science Foundation under awards ATM-0513402/0513421, ANT-034248 and ANT-0424589.

Methods Supplement

Modern climatic forcing: temperature and precipitation

Modern forcing fields of annual surface mass-balance and temperature are specified using simple empirical parameterizations, and then varied in the past depending on ice-core or deep-sea-core time series, similarly to previous studies[6, 7]. Annual surface temperatures (°C) are[33]

$$T = T_m + 34.46 - 0.00914\,h_s - 0.68775\,|\varphi| + 0.1\,\Delta q_a + 10\Delta s/125 \quad (1)$$

where T_m = 0 °C, h_s is elevation (m), $|\varphi|$ is latitude (°S), Δq_a is annual orbital insolation anomaly from present at 80° S (W m^{-2}), and Δs is sea-level departure from present (m) representing atmospheric CO_2 (see equation (6) below). Annual precipitation P (m yr^{-1}) is parameterized via temperature[34]:

$$P = 1.5 \times 2^{(T - T_m)/10} \quad (2)$$

The fraction of precipitation falling as snow, and annual surface melt if any, are computed from T using a positive-degree-day (PDD)[35] method with coefficient 0.005 m per degree-day. A sinusoidal seasonal temperature cycle of amplitude 0.1 Δq_s (°C) is assumed, where Δq_s is January-minus-July 80° S insolation (W m^{-2}). (Very little surface-melt occurs in our simulations, because summer air temperatures remain below freezing everywhere.)

Modern climatic forcing: sub-ice-shelf oceanic melt

A new parameterization of oceanic melt rates is used, based on the degree of protection by islands and bays, and distance to ice-shelf edge.[17] Although simple, it captures basic features of other studies, such as rapid melting near edges,[14, 19, 36, 37] and yields reasonable modern shelf distributions. Modern sub-ice melt M (m yr^{-1}) is

$$M = (1 - z_d)\,[(1 - z_e)\,M_p + z_e\,M_e] + z_d\,M_d \quad (3)$$

where the "deep-ocean" weighting is

$$z_d = \max[0, \min[1, (h_b - 1400)/200]\,] \quad (4)$$

and the "exposed-shelf" weighting is

$$z_e = \max[0, \min[1, (A - 80)/30]\,]\,e^{-D/100} \quad (5)$$

Here max[x, y] indicates the greater of x and y, and min[x, y] indicates the lesser. The 3 modern oceanic melt rates M_p, M_e and M_d in equation (3) are for protected, exposed-shelf and deep-ocean areas, respectively, given by M_p = 0.1 m yr^{-1}, M_e = 5 m yr^{-1}, and M_d = 5 m yr^{-1}. In equations (4) and (5), h_b is bathymetry (m), A is the angle (degrees) subtended by the set of all straight lines from the point in question that reach open ocean without encountering land or grounded ice, and D (km) is the sub-ice distance to the closest open-ocean point. The angle A is the main way we achieve realistic modern ice-shelf edges. Around most major Antarctic shelf-edges today, A is ~90° to 100°; whether this coincidence has a physical basis requires exploration with regional ocean models.

Past climatic forcing: sea level, temperature and precipitation

We need to prescribe long-term variations of sub-ice oceanic melt rates, sea level, air temperature and precipitation over the past 5 Myr. On longer timescales, atmospheric CO_2 levels outside the Plio-Pleistocene range (~180–380 p.p.m.v.), basal sediment changes, and tectonic uplift or subsidence are probably important, but were probably minor through the Plio-Pleistocene. As mentioned above, our Pleistocene-centric parameterizations may underestimate warmth during the early Pliocene ~5–3 Myr ago when CO_2 levels rose to ~380 p.p.m.v. (reference 9).

Sea-level variations have been dominated by Northern Hemispheric ice volume, and are assumed proportional to deep-sea core $\delta^{18}O$ and calibrated as in equation (6). Past variations of Antarctic annual surface temperatures are included in equation (1), proportional to a combination of atmospheric CO_2 (which is represented by $\delta^{18}O$ via sea level in equation (1), since all three are highly correlated in the Pleistocene at least) and the annual 80° S insolation anomaly. Past variations in precipitation depend on air temperature, just as for modern spatial variations (equation (2)).

Past climatic forcing: sub-ice-shelf oceanic melt

The long-term controls of sub-ice-shelf melting are just beginning to be explored.[14, 19, 37] Here we propose a parameterization based on simple reasoning and sensitivity tests of WAIS retreat since 15 kyr ago. This last deglacial retreat is the only well-documented WAIS variation on 10^4-year time scales. It cannot have been driven by surface mass balance, because Antarctic precipitation has increased, not decreased, and there has been negligible surface melt during this time. Model sensitivity tests show that sea-level rise alone, and/or the influence of warming temperatures on ice viscosity and basal sliding, account for only a small fraction of the observed retreat. Therefore, increases in sub-ice melting must have been key. They could reasonably have been driven either by regional Southern Hemispheric orbital insolation changes, or by global-scale far-field influences. Southern Hemispheric insolation is unlikely to have been the dominant driver, because (1) the summertime 80° S anomaly from present was small and negative between 15 and 2 kyr ago, and (2) the annual 80° S anomaly, with minimum at 28.7 kyr ago and maximum at 9.5 kyr ago (reference 20), would have caused retreat to commence too early (before ~19 kyr ago) judging from Ross Sea grounding-line history (~10 kyr ago).[24, 25] This is borne out by sensitivity tests (Supplementary Figure 5) in which austral insolation is used as the sole driver of sub-ice melt, and results over the past 15,000 years are unreasonable. Realistic retreat is obtained only if sub-ice melt varies in step with far-field forcing.

This suggests that sub-ice melt has been controlled not by local forcing or austral insolation, but by far-field climatic influences that vary in step with Northern Hemispheric glacial–interglacial cycles at least since ~2.5 Myr ago. The latter is represented here by a stacked deep-sea-core $\delta^{18}O$ record spanning the past 5 Myr (ref. 18). A small influence of austral summer insolation[20] is added to produce minor observed 20-kyr cyclicity during warm events such as MIS 31.[21] First, a weighting index w_g is defined by

$$w_g = \max[0, \min[2, 1 + \Delta s/85 + \max(0, \Delta q_j/40)\,]\,] \quad (6)$$

where $\delta^{18}O$ is represented by Δs, the sea-level departure from present (m, scaled to $\delta^{18}O$ with last-glacial-maximum 125 m lower than present), and Δq_j is the January 80° S insolation anomaly from present (W m^{-2}). Sub-ice-melt rates for protected, exposed-shelf and deep-sea areas ([M_p, M_e, M_d] respec-

tively, in m yr^{-1}) are specified as [0, 0, 2] for maximum-glacial conditions, [0.1, 5, 5] for modern, and [2, 10, 10] for extreme-interglacial conditions. Then the triplet used in equation (3) to determine M for any past time is

$$[M_p, M_e, M_d] = (1 - w_g)\,[0, 0, 2] + w_g\,[0.1, 5, 5] \quad \text{if } 0 \le w_g < 1 \qquad (7)$$

or

$$[M_p, M_e, M_d] = (2 - w_g)\,[0.1, 5, 5] + (w_g - 1)\,[2, 10, 10] \quad \text{if } 1 \le w_g \le 2 \qquad (8)$$

The modern triplet values are chosen to yield reasonable results for today's Ross and Filchner-Ronne ice shelves. The glacial and warm triplets and the form of w_g in equation (6) are chosen so that the model just attains full-glacial WAIS extents and complete interglacial collapses in long-term simulations and in Figure 1. These values cannot be changed by large amounts without substantial degradation of our results.

Supplementary Materials (following pages)

1. Further Model Description

The ice sheet-shelf model uses a finite-difference Arakawa-C grid, where horizontal velocities (*u,v*) are calculated on separate grids staggered by half a grid box relative to ice thickness (*h)* (Fig. S1)[38].

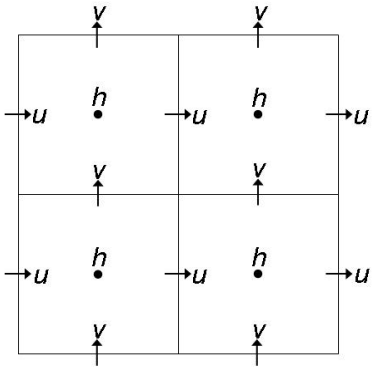

Figure S1. Finite-difference staggered grids in the ice sheet-shelf model. *h* denotes the centers of h-grid boxes, where ice thickness, ice temperatures, and bedrock elevations are calculated. *u* and *v* denote the staggered grid points where horizontal velocity components are calculated.

The equations and method of solution for horizontal velocities are described in detail in Pollard and DeConto[12], including the heuristic, iterative combination of the two sets of scaled equations for terrestrial sheet (Shallow-Ice Approximation, SIA) and marine shelf flows. Although the combined equations can be combined everywhere in the domain, it is faster computationally to only calculate shelf flow in restricted regions – where the basal sliding coefficient is large (slippery beds or floating), or even simpler, only where floating. We have used the latter approach for most simulations here, i.e., allowing shelf flow only where floating. In Supplementary Information (SI) section 8 we show that the long-term results are essentially unchanged by allowing combined flow in grounded areas.

Schoof[5] has shown that to capture grounding-line migration accurately, it is necessary to either resolve the grounding -zone boundary layer at very fine resolution (~0.1 km), or to apply an analytic constraint on the flux across the grounding line. Otherwise, coarse-grid models fail to capture basic aspects of grounding line movement in idealized tests[39,40]. Here, we calculate the flux q_g across model grounding lines as in Schoof[5] (his Eq. 29):

$$q_g = \left(\frac{\overline{A}(\rho_i g)^{n+1}(1-\rho_i/\rho_w)^n}{4^n C'} \right)^{\frac{1}{m'+1}} \left(\frac{\tau_{xx}}{\tau_f} \right)^{\frac{n}{m'+1}} \left(h_g^{\frac{m'+n+3}{m'+1}} \right) \quad \text{(S1)}$$

This yields the vertically

averaged velocity $u_g = q_g/h_g$ where h_g is the ice thickness at the grounding line. The middle term in Eq. (S1) accounts for back stress at the grounding line due to buttressing by downstream islands, pinning points or side-shear, where τ_{xx} is the longitudinal stress across the grounding line from the solution of the shelf-flow equation in the previous iteration, and τ_f is the same quantity in the absence of any buttressing, given by $0.5\ \rho_i\ g\ h_g\ (1-\rho_i/\rho_w)$. Other symbols are as in Schoof[5] and Pollard and DeConto[12]: A is the depth-averaged ice rheological coefficient and n is the Glen-Law exponent, C' is Schoof's[5] basal sliding coefficient and m' the basal sliding exponent, corresponding to $B^{-1/m}$ and $1/m$ here and in Pollard and DeConto[12], due to the reversed form of the basal sliding law (Eq. (S2) below). ρ_i and ρ_w are densities of ice and water respectively, and g is the gravitational acceleration. h_g is interpolated in space by first estimating the sub-grid position of the grounding line between the two surrounding floating and grounded h-grid points. This is done by linearly interpolating height-above-flotation between those two points to where it is zero (cf. Pattyn et al.[41]), linearly interpolating bedrock elevation to that location, and then simply computing the flotation thickness of ice for that bedrock elevation and current sea level.

The velocity u_g is calculated at the grounding-line points on the u-grid, i.e., those with floating ice in one adjacent (left or right) h-grid box and grounded ice in the other (and similarly for v_g on the v-grid). These velocities are imposed as an internal boundary condition for the shelf-flow equations, in effect overriding the large-scale velocity solution at the grounding line. Note that this procedure only considers one-dimensional dynamics perpendicular to the grounding line (as in the 1-D flowline analysis in Schoof[5]). This works naturally with the staggered C-grid (Fig. S1), where the grounding "line" is a continuous series of perpendicular segments of u-direction or v-direction interfaces between h-grid boxes, and u_g (v_g) velocities flow across interfaces running through u-grid (v-grid) points. We neglect spatial gradients parallel to the grounding line, which are not included in the derivation of Eq. (S1); however, they are considered to cause only small second-order effects in typical 2-D flows (C. Schoof, pers. comm.).

We have tested this method of solution in many idealized 1-D flowline tests, similar to those in Schoof[5]. Our goal was to achieve the same grounding-migration results using a coarse grid (~10 to 40 km) with those using very fine-grids (~0.1 km). For grids coarser than ~ 1 km, we find that it is necessary to impose Eq. (S1) as a grounding-line boundary condition. For grids coarser than a few km, we find that an additional rule is necessary, because the outer-solution structure of the grounding zone is not fully captured by the grid:

> If the flux q_g from Eq. (S1) is greater than the large-scale shelf-equation's flux q_m at the grounding line, then u_g (= q_g/h_g) is imposed exactly at the u-grid grounding-line point; conversely if $q_g < q_m$, then u_g is imposed one u-grid box downstream of the grounding-line point. The former is usually associated with grounding-line retreat, and the latter usually with grounding-line advance.

With this rule and 10 to 40 km grids, grounding line retreats and advances are captured correctly in large suites of idealized 1-D flowline tests, many as part of the MISMIP

model intercomparison[39,40]. They include forward and reverse-sloping bedrocks and transient sea-level changes, and our results agree well with those using very fine (~0.1 km) grids and with analytical solutions[5].

Ice thickness advection is treated by an ADI (alternating-direction-implicit) scheme that includes linearized time-implicit tendencies for all SIA terms, and uses time-explicit shelf-flow velocities. Ice temperatures are advected using upstream parabolic interpolation[42], allowing for vertical heat diffusion, geothermal heat flux, basal freezing or melting, and frictional heating by vertical (SIA-flow) shearing, horizontal (shelf-flow) shearing and basal sliding. Geothermal heat flux is set to .070 W m^{-2} for West Antarctica, and .0546 W m^{-2} elsewhere[43]. Basal sliding velocities u_b are related to basal stress τ_b as in Pollard and DeConto[12]:

$$\vec{u}_b = B\left|\tau_b\right|^{m-1}\vec{\tau}_b \qquad \text{(S2)}$$

with $m = 2$. Where basal temperatures are at the pressure melting point, the basal sliding coefficient B is set to either 10^{-10} m a^{-1} Pa^{-2} (typical of hard bedrock) or 10^{-6} m a^{-1} Pa^{-2} (typical of deformable sediment). Sediment is assumed to exist where today's rebounded ice-free BEDMAP[1] topography lies below sea level, as a simple attempt at prescribing the large-scale sediment distribution. Additionally, for all runs shown here, B is set to an intermediate value of 10^{-8} m a^{-1} Pa^{-2} in a rectangle roughly corresponding to the Pine Island/Thwaites drainage basin, to achieve more realistic modern grounding lines in that region of the Amundsen Sea. Further adjustments to West Antarctic's B values in sensitivity tests are discussed in SI section 7. As basal temperatures fall below the pressure melt point from 0 to -0.5°C, B is ramped towards essentially zero (10^{-20}, linearly with respect to log(B)), i.e., no sliding if grounded ice is frozen to the bed. However, no such temperature adjustment to B is made at grounding lines, under the assumption that basal ice in the grounding-line boundary layer is always very close to melting.

2. Simulation of Modern Antarctica

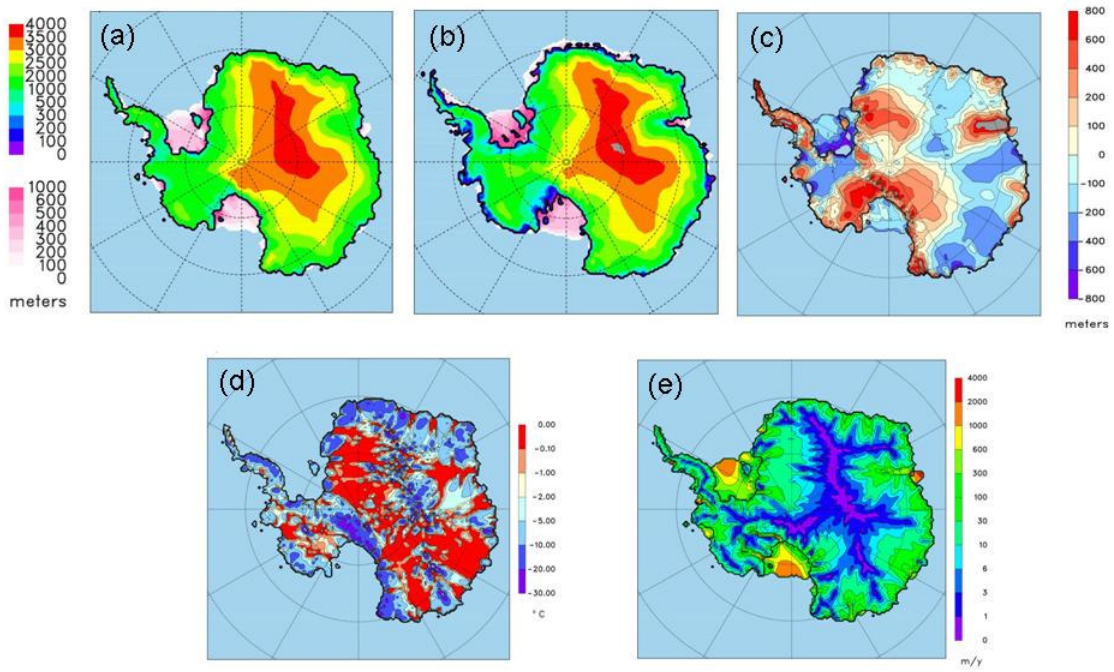

Figure S2. (**a**) Model ice elevations (grounded) and thicknesses (floating), for modern (0 ka) in the nominal run shown in Fig. 2b. (**b**) As (a) for modern observed Antarctica[1]. (**c**) Differences a-b, model minus observed. (**d**) Model basal temperatures relative to the pressure melt point (ºC, red ≈ melting) at 0 ka. (**e**) Model ice surface speeds (m y^{-1}) at 0 ka.

General error magnitudes in modern ice elevations (Fig. S2c) are on the same order as those found in other Pleistocene models[6,7]. There are large errors over the Lambert Graben/Prydz Bay (~80ºS, 70ºE) where the model grounding line is too far advanced down the bay, and conversely for the innermost Ronne Ice Shelf. Elsewhere, the agreement with modern grounding-line locations is good, especially in the Ross Embayment. The two largest islands (Roosevelt and Berkner) under the major shelves are captured. Ice elevations are too high over much of western WAIS (grounded Siple Coast and Rockefeller Plateau), perhaps due to too much bed friction with not enough bed area reaching the melt point, resulting from the model's lack of basal hydrology and liquid water flowing originating upstream[44]. Floating ice thicknesses in the Ross and Filchner-Ronne shelves are somewhat thinner than observed. Both of these errors are partially corrected in sensitivity experiments described below in SI sections 6-7. Future work will aim at further improving these aspects, focusing on basal hydrology, sediment distribution, and the long-term evolution leading up to the modern snapshot at 0 ka.

Supplementary Materials

Model ice speeds (Fig. S2e) generally compare well with modern balance velocity maps and measurements[45,46]. In both panels (d) and (e), hints of poorly resolved ice "streams" are seen in the Siple Coast and Prydz Bay regions; these are resolved much better in the higher-resolution nested run shown in Fig. 3f and Supplementary Videos V3-4. Simulated ice velocities of the modern Byrd Glacier (80.3ºS, 160ºE) and some of the Siple streams in Fig. 3f are somewhat faster than observed[47-49], perhaps because of neglect of longitudinal stresses or incorrect basal stiffness.

3. Simulated Conditions at Specific Points in the Ross Embayment

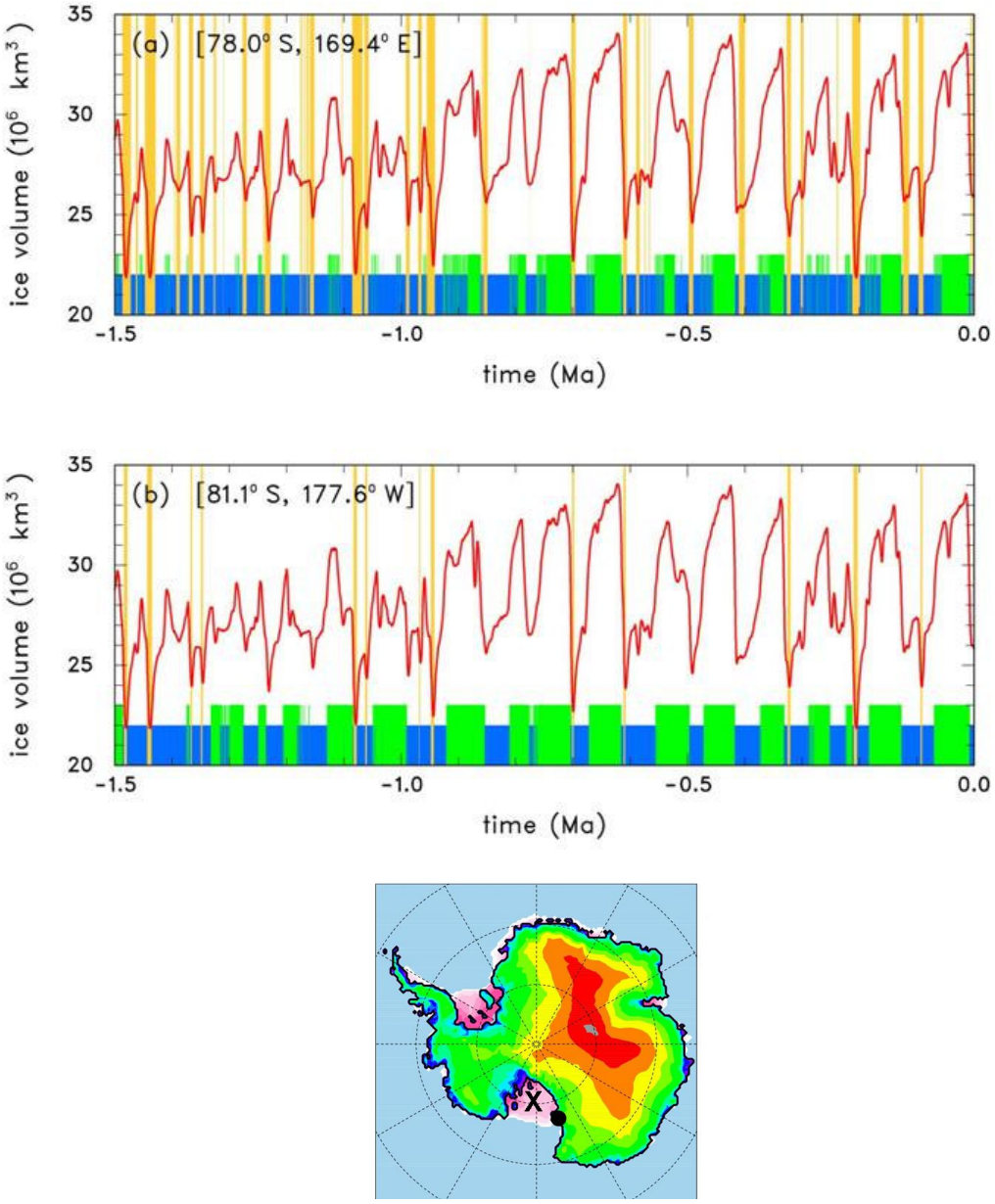

Figure S3. Total Antarctic ice volume for the last 1.5 Myr of our nominal long-term simulation. (**a)** Lower colored boxes indicate conditions at a single location one grid box to the east of the ANDRILL AND-1B core[11] (black dot in map) in McMurdo Sound. Yellow = open ocean, blue = floating shelf, green = grounded ice. The eastward shift was made to avoid poorly resolved Ross Island shorelines. (**b)** Same as (a) except for grid location (81.1ºS, 177.6ºE, black X in map) in the central region of the Ross Embayment.

Supplementary Materials

The upper panel (a) in Fig. S3 is the same as in Fig. 2c, except the yellow boxes (open ocean) are extended upwards to show correlations with ice-volume minima. In the lower panel, open-ocean events at the more central Ross-Sea location are more infrequent, and with few exceptions occur only for near-complete WAIS collapses (total ice volume < ~23×10^6 km^3). A core drilled at this site would have the potential of uniquely identifying WAIS collapses, assuming other requirements such as sediment preservation are met.

4. Marine Isotope Stage 31

Sediment cores near Ross Island[11, 21] and elsewhere around Antarctica[50] indicate strong circum-Antarctic warming during Marine Isotope Stage 31 ~1.08 to 1.06 Ma. Drastic ice-shelf retreat and seasonally open water around Ross Island at this time[11,21] coincide with one of the strongest austral summer insolation anomalies of the Pleistocene[20]. The model time series around MIS-31 (Fig. 2c) has a distinct precessional (~20 kyr) component due to the influence of austral summer insolation, and agrees well with the phase of the 20 kyr cyclicity in off-shore records[21]. The snapshot at 1.079 Ma (Fig. 3b) shows peak collapse of nearly all marine ice in West Antarctica. Although the actual degree of collapse is not known, the retreat of shelf ice far southward of Ross Island agrees with data[10, 11]. In Global Climate Model (GCM) simulations of MIS-31 climate, with the Ross Ice Shelf removed and with ocean melting under sea ice increased to match our sub-ice-shelf parameterization[51], we find ~4ºC summer warming and open ocean near Ross Island in full agreement with interpretations based on diatom assemblages[21]; however, this warming is insensitive to the size of WAIS specified in the GCM, so the results do not shed light on the degree of collapse.

5. Sensitivity Experiments: Southern Hemispheric Solar Insolation Forcing

Our use of deep-sea-core benthic $\delta^{18}O$ as the main long-term forcing is empirical and pragmatic. The $\delta^{18}O$ time series has two properties that are consistent with the new AND-1B record of Antarctic response[11]: its higher-frequency fluctuations mainly have ~40 kyr periodicity, and it has a long-term cooling trend over the last 5 Myr from the early-to-mid Pliocene (~5 to 3 Ma) to the late Pleistocene glacial cycles (~1 to 0 Ma). The fact that our model response mirrors these basic features is not surprising; instead, the main substantive outcome of this study is that (i) the simulations are in reasonable agreement not only with AND-1B, but also with observed last glacial (15 ka) to modern extents, and implied drastic WAIS retreats in a few previous interglacials, and (ii) this can be achieved with plausible values of past and present sub-ice oceanic melt rates.

However, our use of $\delta^{18}O$ to drive long-term forcing variations, with an additional slight influence of austral summer insolation, is really a hypothesis. It is clearly testable by further work with global climate and regional ocean dynamical models. Here, as a very crude test of alternate forcings, we performed two sensitivity tests using only Southern Hemispheric insolation as long-term forcing, with no $\delta^{18}O$ influence (Fig. S5). Using annual insolation anomalies (solid blue curve), the last WAIS deglacial retreat is now quite unrealistic, beginning and ending too early (~20 to 10 ka) compared to observed (~10 to 3 ka[24,25]). Using summer insolation anomalies (dashed blue curve), similar problems arise for the last deglacial retreat. This bears out our reasoning in the Methods section, that the observed timing of the last glacial maximum and retreat of WAIS must have been forced primarily by far-field influences correlated with benthic $\delta^{18}O$.

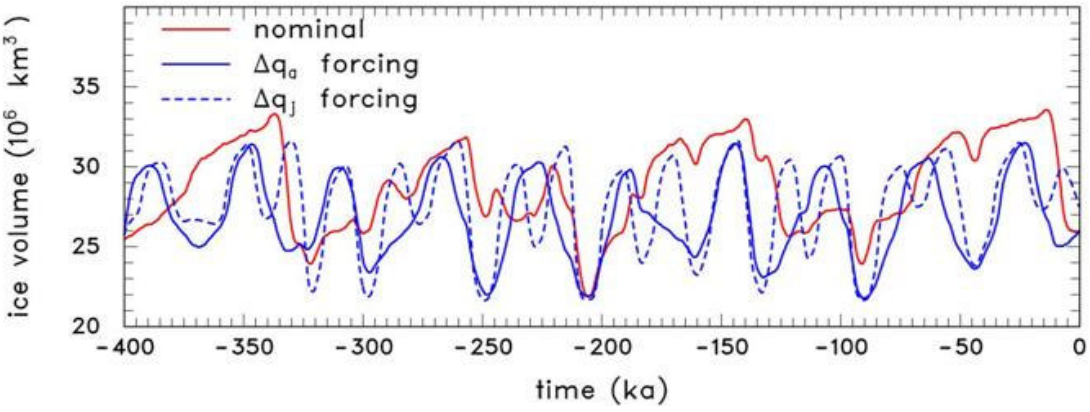

Figure S5. Simulated Antarctic ice volume for the last 400 kyr. **Red:** nominal long-term simulation. **Solid blue:** with austral *annual mean* insolation anomaly at 80ºS (Δq_a, W m^{-2}) instead of deep-sea-core ($\delta^{18}O$) as the main long-term forcing of sub-ice melt, i.e., with the $\Delta s/85$ term in Eq. (6) of the Methods section replaced by (0.1 Δq_a - 0.3) / 0.9. **Dashed blue:** with austral *summer* (January) insolation anomaly at 80ºS (Δq_j, W m^{-2}), i.e., with $\Delta s/85$ in Eq. (6) replaced by (0.1 Δq_j - 1) / 5. These expressions are adjusted to maintain roughly the same mean ice-sheet sizes and peak-to-peak amplitudes as in the nominal run.

6. Sensitivity Experiment: Last Deglacial History

The deglacial history of Antarctica over the last ~15,000 years is relatively well known, and provides valuable data for model validation. In particular, the sequence of grounding line retreat across the Ross Embayment has been deduced from local geologic evidence as similar to a "swinging gate", with fairly smooth retreat from near-continental-shelf edges ~15 ka to close to present after ~3 ka[24,25]. In our nominal long-term run, the model's Ross-Embayment retreat resembles a swinging gate (shown in Supplementary Video V1), but is too sudden and occurs mostly between 10 ka and 8 ka.

The retreat is noticeably improved in a sensitivity experiment with increased buttressing of ice shelves. This experiment was motivated by several small ice rises observed just downstream of the modern Siple Coast grounding line (Horgan and Anandakrishnan[52] and H. Horgan, pers. comm.), which are not resolved by the 40 km grid. We added a parameterization of sub-grid pinning by small bedrock rises, in which additional basal stress is applied at the bottom of floating ice for water column thicknesses $h_w \leq 300$ m; i.e., the basal sliding coefficient is ramped linearly from 15% of the grounded-ice value (for $h_w = 0$) to no resistance (for $h_w \geq 300$). This by itself would cause buttressing to increase and grounding lines to advance unrealistically, so to compensate, we increased the grounding-line fluxes given by Eq. (S1) by a factor of 10. This leaves grounding-line locations mostly unchanged, and causes a general thickening of shelf ice, improving the underestimation of modern thicknesses in the nominal run (actually overcorrecting for the Ronne). Loosely speaking, these modifications increase the amount of "compression" in the major ice shelves between the grounding-line input flux and the downstream resistance.

The modeled sequence through the last deglaciation (after a 400 kyr run) is shown in Fig. S6. The sequence of grounding-line retreat in the Ross Embayment is now much smoother and lasts from ~10 ka to 2 ka, in much better agreement with observations[24,25].

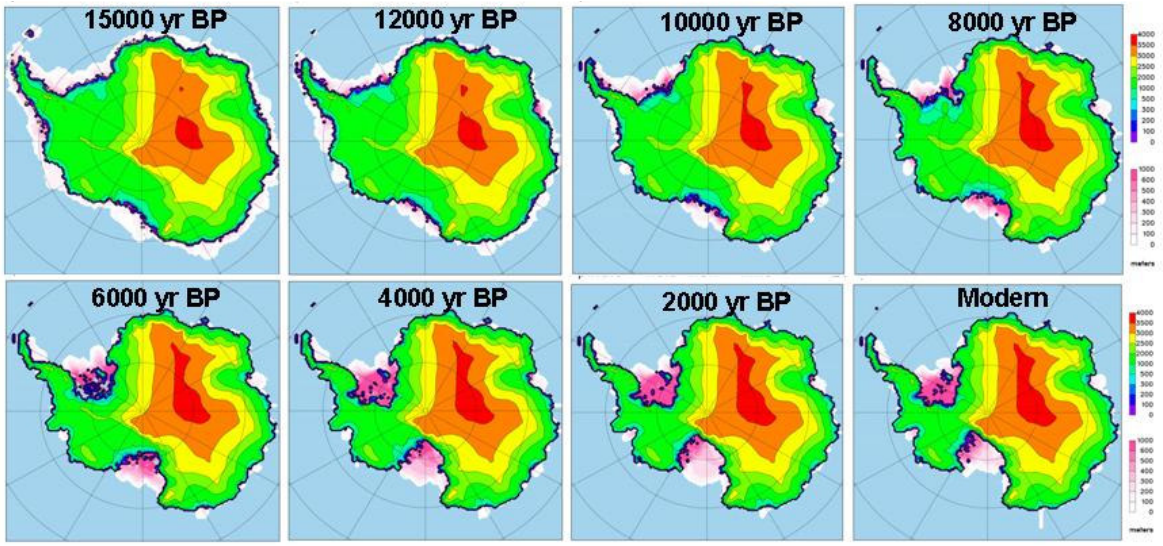

Figure S6. Snapshots of ice elevations (grounded) and thicknesses (floating) through the last deglaciation in the sensitivity run described above with sub-grid ice-shelf pinning and increased grounding-line flux coefficient (see text). These changes considerably improve the realism of grounding-line retreat in the Ross Embayment.

7. Sensitivity Experiment: West Antarctic Ice Sheet Profiles

The largest departure from modern observed conditions in our nominal simulation is the overestimation of ice thicknesses over WAIS (SI section 2). This problem is common to earlier models[6, 7] and has been ascribed to underestimated basal sliding, perhaps due to insufficient lubrication or too much bed area below freezing[44]; also there may be insufficient overall transport by ice streams, which are barely resolved with a 40 km grid. The overestimation of ice thickness is exacerbated at the last glacial maximum (15 ka for Antarctica), when expanded ice cover over the Ross Embayment remained thin far inland from the grounding line, only a few hundred meters thicker than modern in many areas[53,54].

This study does not resolve the problem, which we regard as a major future challenge in this field. Its resolution will likely require better knowledge of sediment vs. bedrock and frozen vs. thawed bed distributions under WAIS, and better understanding of the large-scale role of ice streams (cf. SI section 8). Our main concern here is that long-term WAIS evolution and our 5 Myr results do not depend acutely on details of WAIS sediment distributions or ice profiles. To test this, we performed several sensitivity experiments with increased basal sliding coefficients under WAIS that produce more realistic (lower) ice profiles. One such experiment is described below, with little change in the long-term ice sheet variations (Fig. S7A). This suggests that the main results of this paper are robust, and will not be changed substantially by further tuning of bed conditions to reduce modern biases.

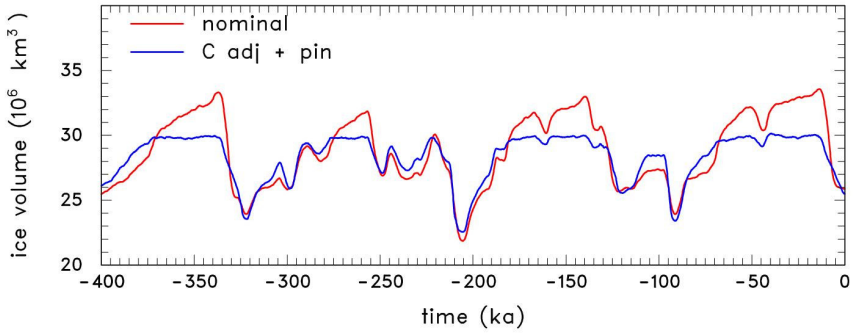

Figure S7A. Red: Total ice volume in last 400 kyrs of the nominal model simulation. **Blue:** Sensitivity experiment with adjustments to WAIS basal sliding coefficients, and also sub-grid ice-shelf pinning (see text).

The main change in Fig. S7A (blue curve) is an increase in the basal sliding coefficient B over WAIS sediment areas to 10^{-5} (from 10^{-6}) m a^{-1} Pa^{-2}, except in the Filchner-Ronne drainage area where it is kept at 10^{-6}. In addition, over Siple Coast drainages, some sliding is permitted for frozen beds, with B reduced only to 10^{-7} m a^{-1} Pa^{-2} (not to ~zero; cf. Parizek et al.[44]). This run also includes the sub-grid pinning parameterization described in SI section 6. The time series of total ice volume is much the same as the nominal run, except that maximum glacial volumes are capped at ~30 x 10^6 km^3. The

larger nominal values are due to ~km thicker ice over much of WAIS during glacial periods.

Over much of the Siple Coast region, grounded ice elevations in the new simulation are ~500 m lower (Figs. S7B amd S7C). Upstream from the modern grounding line, elevations in the new run are a few hundred to several hundred meters higher at 15 ka than modern, still somewhat more than observed at some locations[53,54], but more realistic than the larger 15 ka vs. modern differences in the nominal run.

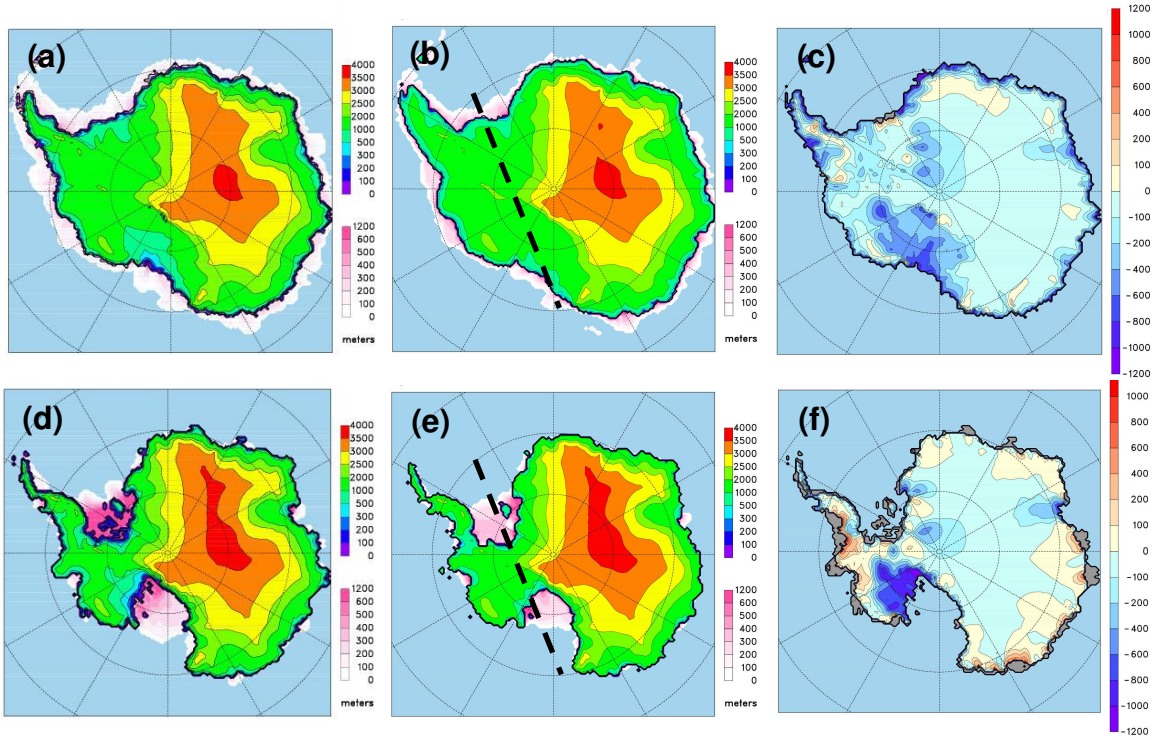

Figure S7B. **(a)** Ice elevations (grounded) and thicknesses (floating) at 15 ka, in a sensitivity test with adjustments to the basal sliding coefficient under WAIS areas, and also sub-grid ice-shelf pinning (see text). **(b)** At 15 ka, in the nominal model. **(c)** Difference (a minus b). **(d) to (f)** Same as (a) to (c) except for modern. The cross section for Fig. S7C is shown in (b) and (e) as a thick dashed line.

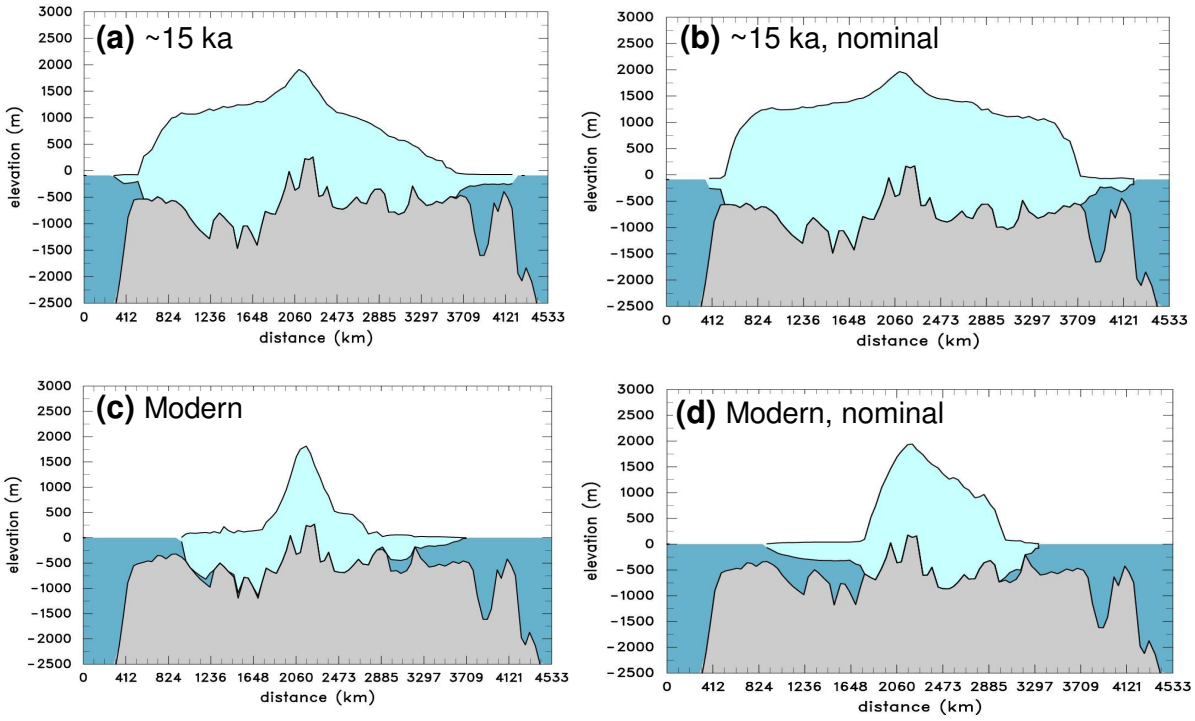

Figure S7C. Cross sections of ice and bedrock through WAIS, from the Weddell Sea (left) to the Ross Sea (right), [70ºS,40ºW] to [70ºS,178ºE] as shown in Fig. S7B(a,b,d,e). **(a)** At ~15 ka, in a sensitivity experiment with adjustments to the basal sliding coefficient under WAIS areas, and also sub-grid ice-shelf pinning (see text). **(b)** At ~15 ka, in the nominal model. **(c) and (d)** Same as (a) and (b) except for modern.

8. Sensitivity Experiment: Combined Flow Equations in Grounded Areas

As described in SI section 1, for efficiency in most runs we do not use the heuristically combined sheet (SIA) and shelf-flow equations everywhere[12], but apply them separately to grounded and floating regions respectively. This simplification is likely to have most impact in the transition zone upstream of grounding lines, where longitudinal stresses in ice streams may be important for the large-scale evolution. Without longitudinal stresses, the modern Siple Coast network of ice streams is simulated quite well in our 10-km nested runs (Fig. 3, and videos V3–V4) and even somewhat in our 40 km runs, and stems from the positive feedback between basal sliding, frictional heating and thawing at the bed[55]. However, the role of ice streams and the level of ice-stream detail needed for modeling long-term ice-sheet evolution are not well known, and are important ongoing research areas. Here, we take a step in this direction, by performing a sensitivity run with the heuristic sheet-shelf-flow iterative combination applied in grounded as well as floating regions. It would be too computationally expensive to do this over the entire domain (and wasteful, because in our coarse-grid model, non-SIA stretching flow is negligible over most of EAIS with low basal sliding coefficients $B = 10^{-10}$ m a^{-1} Pa^{-2}). Instead, we apply the combination only where $B > 0.5\ 10^{-8}$ m a^{-1} Pa^{-2}, which includes all thawed sediment beds (much of WAIS). This modification is in addition to those for the sensitivity tests described in SI sections 6 and 7. Results for the last 400 kyr are shown in the figures below.

The time series of ice volume (Fig. S8A), mainly reflecting variations in WAIS extent, is essentially unchanged by the inland combined calculations, both for interglacial and glacial states. With this modification, grounding lines in the Weddell and Ross embayments tend to be more advanced, as seen for modern in Fig. S8B. However, the amount of grounding-line shift is relatively small, and is typical of those induced by many small parameter changes in the model that produce only minor changes in the long-term evolution.

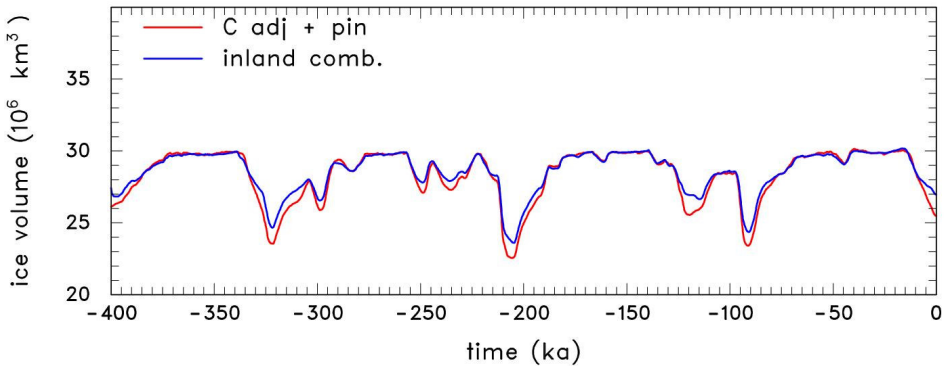

Figure S8A. Red: Total ice volume in the previous sensitivity experiment described in SI section 7 with adjusted WAIS basal sliding coefficients and sub-grid ice-shelf pinning. **Blue:** With those changes, and also with combined sheet-shelf-flow calculations in regions with basal sliding coefficient $B > 0.5\ 10^{-8}$ m a^{-1} Pa^{-2} (which includes most of inland WAIS).

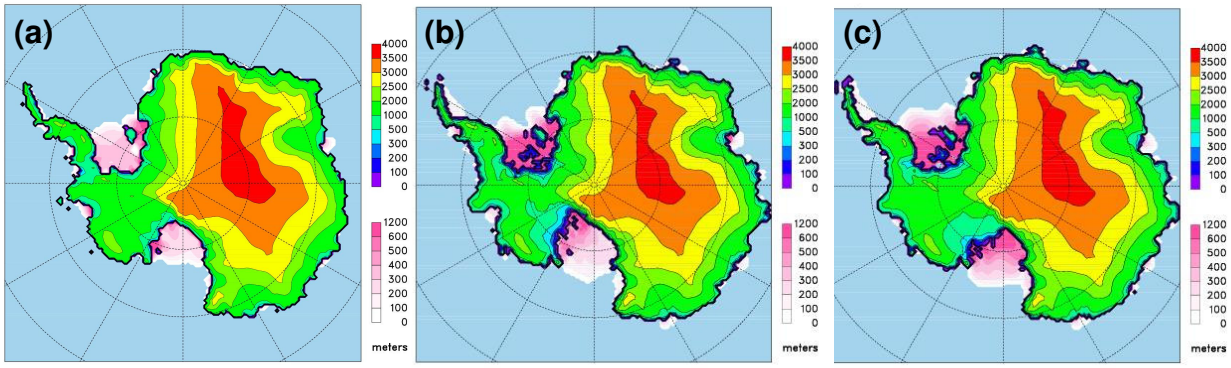

Figure S8B. Snapshots of modern ice elevations (grounded) and thicknesses (floating). **(a)** In the nominal model simulation. **(b)** In the previous sensitivity experiment described in SI section 7 with adjusted WAIS basal sliding coefficients and sub-grid ice-shelf pinning. **(c)** With those changes, and also with combined sheet-shelf flow calculations in regions with basal sliding coefficient $B > 0.5\ 10^{-8}$ m a^{-1} Pa^{-2} (which includes most of inland WAIS).

SUPPLEMENTARY REFERENCES

38. Rommelaere, V. & Ritz, C. A thermomechanical model of ice-shelf flow. *Ann. Glaciol.* **23**, 13-20 (1996).
39. Schoof, C., Hindmarsh R. & Pattyn, F. Benchmarks and intercomparison program for marine ice sheet models. Abstract EGU2007-A-04644, *European Geosciences Union,* General Assembly, Vienna, http://homepages.ulb.ac.be/~fpattyn/mismip and http://meetings.copernicus.org/egu2007/annotation.html (2007).
40. Pollard, D. & DeConto, R. Grounding line behavior in a heuristally coupled ice-sheet shelf model. Abstract EGU2007-A-03103, *European Geosciences Union*, General Assembly, Vienna, http://meetings.copernicus.org/egu2008/annotation.html (2008).
41. Pattyn, F., Huyghe, A., De Brabander S. & De Smedt, B. The role of transition zones in marine ice sheet dynamics. *J. Geophys. Res.-Earth Surface*, **111**, F02004, doi:10.1029/2005JF000394 (2006).
42. Farrow, D.E. & Stevens, D.P. A new tracer advection scheme for Bryan and Cox type ocean general circulation models. *J. Phys. Oceanogr.* **25**, 1731-1741 (1995).
43. Pollard, D., DeConto R. M. & Nyblade, A. A. Sensitivity of Cenozoic Antarctic ice sheet variations to geothermal heat flux. *Glob. Planet. Change* **49**, 63-74 (2005).
44. Parizek, B.R., Alley, R. B. & Hulbe, C. L. Subglacial thermal; balance permits ongoing grounding-line retreat along the Siple Coast of West Antarctica. *Ann. Glaciol.* **36**, 251-256 (2003).
45. Bentley, C.R., Rapid sea-level rise from a West Antarctic ice-sheet collapse: a short-term perspective. *J. Glaciol.* **44**, 157-163 (1998).
46. Huybrechts, P., Steinhage, D., Wilhelms F. & Bamber, J. Balance velocities and measured properties of the Antarctic ice sheet from a new compilation of gridded data for modelling. *Ann. Glaciol.,* **30***,* 52-60 (2000).
47. Whillans, I. M., Chen, Y. H., Vanderveen C. J. & Hughes, T. J. Force Budget .3. Application to 3-Dimensional Flow of Byrd Glacier, Antarctica. *J. Glaciol.* **35**, 68-80 (1989).

48. Joughin, I. & Tulaczyk, S. Positive mass balance of the Ross Ice Streams, West Antarctica. *Science* **295**, 476-480 (2002).
49. Rignot, E. *et al*. Recent Antarctic ice mass loss from radar interferometry and regional climate modelling. *Nature Geoscience* **1**, 106-110 (2008).
50. Villa G., C. *et al*. A Pleistocene warming event at 1 Ma in Prydz Bay, East Antarctica; Evidence from ODP site 1165. *Palaeogeogr., Palaeoclim., Palaeoecol,* **260**, 230-244 (2008).
51. DeConto, R. *et al.*. Antarctic climate-cryosphere response to extreme orbital forcing during Marine Isotope Stage 31. *EOS Transactions*, American Geophysical Union **88**, Fall Meeting Suppl., Abstract PP41F-07, http://www.agu.org/meetings/fm07/waisfm07.html (2007).
52. Horgan, H. J. & Anandakrishnan, S. Static grounding lines and dynamic ice streams: Evidence from the Siple Coast, West Antarctica. *Geophys. Res. Lett.*, **33**, L18502, doi:10.1029/2006GL027091 (2006).
53. Waddington, E. D. *et al.* Decoding the dipstick: Thickness of Siple Dome, West Antarctica, at the Last Glacial Maximum, *Geology* **33**, 281-284 (2005).
54. Ackert, R. P., Mukhopadhyay, S., Parizek B. R. & Borns, H. W. Ice elevation near the West Antarctic Ice Sheet divide during the last glaciation. *Geophys. Res. Lett.* **34**, L21506, doi:10.1029/2007GL031412 (2007).
55. Payne, A. J. A thermomechanical model of ice flow in West Antarctica. *Clim. Dyn.* **15**, 115-125 (1999).
56. Siegert, M. J. *et al.* Ice flow direction change in interior West Antarctica. *Science* **305**, 1948-1951 (2004).

Supplementary Materials

SUPPLEMENTARY VIDEO LEGENDS

Video V1. This animation shows model surface elevations of grounded ice and thicknesses of floating ice (m), every 1000 years through the last 400 kyr of the long-term simulation shown in Fig. 2b. The major ~100 kyr glacial-interglacial cycles are prominent. As discussed in the text, there is a tendency for WAIS to vary "one-dimensionally", i.e., with its different sectors usually retreating and expanding in unison, resulting in just one configuration for a given total ice volume. Both this video and V2 show that collapsed WAIS states are relatively short lived, and that transitions into and out of them are usually rapid, taking one to a few thousand years.

Video V2. Same as V1 except every 2000 years for the period 1.7 Ma to 0.6 Ma, which includes the Marine Isotope Stage 31 event ~1.08 to 1.06 Ma.

Video V3. This animation shows surface ice velocities (m y^{-1}) every 50 years in the higher-resolution (10 km) nested simulation for modern conditions (Fig. 3f,i). For nested runs, the model physics are identical to the continental model. Boundary conditions of ice thickness and velocity at the edges of the domain, and initial conditions in the interior are obtained by interpolating the course-grid (40-km) results for 0 ka. Over the 8800 years of this nested run, ice and grounding-line configurations continue to evolve away from the initial 0 ka "snapshot" state, which is not consistent with the fixed 0-ka boundary conditions applied at the edges. Also, the finer resolution does change the model behavior somewhat, such as (unrealistically) greater extents of ice-shelf edges. Nevertheless, as also seen in Fig. 3f, Siple Coast ice streams are surprisingly well resolved, and the network sometimes bears some correspondence to the actual streams. Although the placement of the streams is loosely controlled by shallow ridges and valleys in the prescribed bed topography[1], the narrowness of the streams, network morphology, and the position of the grounding line itself are primarily a consequence of the model physics. Over the course of this animation, the Siple Coast network is highly dynamic, with ice streams first becoming established and then stagnating and restarting on ~10^3-year time scales. Similar behavior was found in a WAIS ice flow model by Payne[55], and is reminiscent of the recent stagnation of the Kamb Ice Stream (formerly C) and other century-to-millennial scale switching[31,56].

Video V4. Same as V3 except showing temperatures at the ice-bed interface relative to the pressure melt point (ºC). Red shows the base essentially at the melt point, where basal sliding can occur. Below -0.5ºC, basal sliding is zero. The beds of active Siple Coast ice streams and their source regions are at the melt point, and are frozen over much of the intervening areas[55]. The same is true for major outlet glaciers flowing through the Transantarctic Mountains.